Research Article **Open Access**

Giuseppe de Vito* and Vincenzo Piazza

Fast signal analysis in Rotating-Polarization CARS microscopy

Abstract: Rotating Polarization Coherent Anti-Stokes Raman Spectroscopy (RP-CARS) is a novel approach to CARS microscopy that takes advantage of polarization-dependent selection rules in order to gain information about molecule orientation anisotropy and direction within the optical point spread function. However, in the original implementation of this technique, the lock-in amplifier-based acquisition was quite time demanding. Here we present a new software-based approach that permits a great speed-up in the RP-CARS images acquisition process.

***Corresponding Author: Giuseppe de Vito:** Center for Nanotechnology Innovation @NEST, Istituto Italiano di Tecnologia, Piazza San Silvestro 12, I-56127, E-mail: giuseppe.devito@iit.it
***Corresponding Author: Giuseppe de Vito:** NEST, Scuola Normale Superiore, Piazza San Silvestro 12, I-56127 Pisa, Italy, E-mail: giuseppe.devito@sns.it
Vincenzo Piazza: Center for Nanotechnology Innovation @NEST, Istituto Italiano di Tecnologia, Piazza San Silvestro 12, I-56127

1 Introduction

CARS (Coherent anti-Stokes Raman Scattering) microscopy is an innovative and versatile optical technique based on the coherent generation of a strong resonant Raman anti-Stokes radiation by the target molecules [1]. This technique permits the imaging of fixed and live biological specimina without the need of fluorescent probes. In this way it is possible to avoid the alteration of the target molecule or of the cell as a whole induced by the fluorophore *per se* or by the labeling procedure [2]. The CARS signal conveys rich spectral information, like traditional Raman microimaging, therefore it provides an excellent chemical selectivity. However, unlike Raman microimaging, the signal intensity is several orders of magnitude stronger, thus enabling imaging at high frame rates and low laser power levels [3–5]. The CARS process itself is a four-wave mixing process in which the frequency difference of a pair of incoming photons ("pump" and "Stokes") matches exactly the vibrational frequency of the molecular bond of interest. The molecular vibrational mode thus excited is coherently probed by a third photon that stimulates anti-Stokes emission yielding the signal which is finally detected [6].

In presence of molecular orientation anisotropy in the sample, CARS images often display artifacts due to polarization-dependent selection rules that affect the measured intensity with respect to the alignment between the polarization plane of the incident light and the main orientation plane of the molecular bonds. A few methods were proposed in the literature to reduce these polarization-dependent artifacts. In Ref. [7] a combination of a half-wave plate and a quarter-wave plate is exploited for both the pump-and-probe beam and the Stokes beam in order to make them circularly polarized. Other authors achieved similar results with linearly polarized pump-and-probe and Stokes beams by acquiring two images of the same field rotating the polarization plane of 90° after the first image and mathematically post-processing them [8].

A recent article [9] presented a novel approach, named "Rotating Polarization (RP) CARS", to take advantage of these effects – similarly to what other authors demonstrated with four-wave mixing microscopy [10], two-photon fluorescence, second harmonic generation [11], and CARS [12] – rather than suppressing them. In this approach the authors continuously rotated the orientation of the polarization plane of the incident light with a rotating waveplate and then for each image pixel, they analyzed the orientation dependence of the signal intensity using a lock-in amplifier. This allowed measuring the average-orientation plane of the molecular bond of interest (CH_2 in myelin) and the degree of this spatial anisotropy in the point-spread-function volume for each pixel. However this approach is quite time demanding, as for each pixel it is necessary to acquire several rotations of the waveplate before being able to proceed to the next pixel of the image. Here we present a novel approach that, substituting the hardware lock-in amplifier with a software algorithm, is able to considerably speed up the acquisition process by overcoming the need for sequential pixel acquisition.

2 Results and discussion

The RP-CARS setup employed is shown in Fig. 1. The 800-nm pump-and-probe degenerate beam from a Ti-Sa pulsed laser (fs Laser), shown as red lines, is split by a beam splitter (BS) and routed to the supercontinuum generator (SCG, photonic-crystal fiber SCG-800 Newport [13]) and, through a 3-nm bandpass filter (3-nm BP) centered at 800 nm (approximately 750-fs pulses) and a telescopic beam expander (BE), to the rotating $\lambda/2$ retarder (R-$\lambda/2$). The linearly-polarized broadband (wavelength range: from 450 nm to 1200 nm) Stokes radiation (green lines) is filtered by a 1000 nm-1100 nm combination of shortwave and longwave pass filters (BP2) in order to excite the symmetric stretch vibration of the CH_2 bonds, delayed by a delay line (DL) in order to achieve the temporal overlap between the pulses, transformed into circularly polarized light by an achromatic $\lambda/4$ retarder ($\lambda/4$), and recombined with the 800-nm radiation by means of a 818-nm long-pass dichroic mirror (D). Stokes radiation chirp was minimized by carefully tuning the power and chirp of the input pulse [14]. A second $\lambda/4$ retarder in the pump and probe path allows compensating for polarization distortions caused by D. The two are then routed to the high-Numerical Aperture (NA) lens (Obj, Zeiss EC Plan-NEOFLUAR, 40X, 1.3 NA) of an inverted microscope through a pair of galvo-scanning mirrors, a scan lens and a tube lens. CARS signal is collected from the sample (S) in the trans-direction by a condenser lens (Cond, NA=0.55), edge-filtered to remove the pump photons, band-pass filtered (BP, filter centered at 650 nm and a full width at half maximum of 10 nm) to select the Raman band of the CH_2 bonds here of interest at 2850 cm^{-1}, and routed to a red-sensitive photomultiplier tube (PMT). CARS signal is collected also in the epi-direction by the mean of a dichroic mirror situated between the scan lens and the tube lens. This last signal is focused by a lens, filtered in the same way as the trans-direction signal (BP), and acquired by a second red-sensitive photomultiplier tube (PMT). M0 and M1 are silver-coated mirrors. The output of the PMTs is acquired by a digital acquisition board (DAQ) and then analyzed by a PC. The reference phase and frequency for the software analysis is generated by a Hall sensor (HS) in close proximity to the rotor of the brushless motor that rotates R-$\lambda/2$. The Hall sensor produces two TTL pulses per rotation, therefore the pulse angular frequency corresponds to the polarization-plane angular frequency and is twice that (ω_R) of the R-$\lambda/2$.

In order to obtain a fast acquisition process, we elaborated a software approach that mimic in some aspects

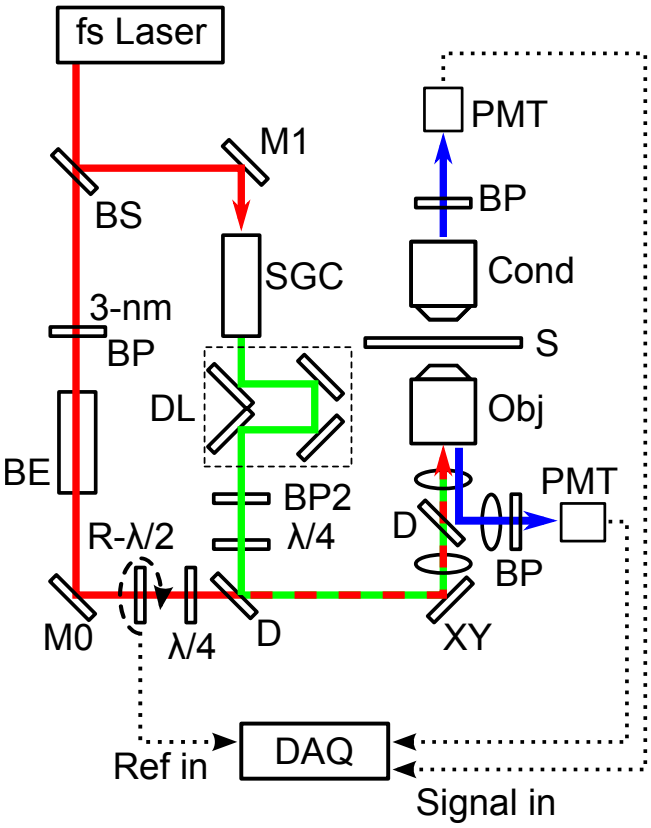

Fig. 1. Schematic representation of the employed RP-CARS setup. Legend: beam splitter (BS), supercontinuum generator (SCG), 3-nm bandpass filter (3-nm BP), telescopic beam expander (BE), rotating $\lambda/2$ retarder (R-$\lambda/2$), combination of shortwave and longwave pass filters (BP2), delay line (DL), achromatic $\lambda/4$ retarders ($\lambda/4$), 818-nm long-pass dichroic mirror (D), microscope objective (Obj), galvo-scanning mirrors (XY), sample (S), condenser lens (Cond), 650-nm band-pass filters (BP), photomultiplier tubes (PMT), silver-coated mirrors (M0, M1), digital acquisition board (DAQ). Red line: 806 nm laser light; green line: Stokes laser light; blue line: CARS signal.

a hardware lock-in amplifier and we implemented the algorithm with the LabVIEW programming language (LabVIEW 2010 SP1, National Instruments). Images are acquired by raster-scanning the laser spot onto the sample using a pair of galvanometric mirrors and digitizing under computer control the output of the PMT and the output of the HS by means of a fast digital acquisition board (USB-6366, National Instruments). In the following we shall refer to lines of pixels along the fast-scan direction as “columns” and perpendicular to it as “rows”. Each column of the image is scanned multiple times (N) while the R-$\lambda/2$ is rotating and the corresponding signal digitized after moving the laser spot to the next column.

For each pixel, the signals from the PMT and from the HS are acquired with an integration time of T_p. Care has to be taken in order to choose the time needed to scan the col-

umn, $T_L = T_p n_y$ (where n_y is the number of pixels per column) to be much shorter than the rotation period so that each pixel of the column is sampled many times for each rotation period in order to satisfy the Nyquist sampling theorem but, at the same time, long enough to account for the limited dynamics of the galvo mirror (400-Hz resonant frequency). Additionally, the total acquisition time of the column, $2NT_L$ (here the factor of two accounts for the fact that the columns are always scanned in the same direction and the galvo mirror has to go back to the top of the column before starting a new scan), has to be long enough to encompass a few rotations of the R-$\lambda/2$.

This acquisition procedure yields two multidimensional arrays, $S(x, y, i)$ and $H(x, y, i)$, containing the digitized values of the outputs of the PMT and of the Hall sensor respectively. Here x and y label the columns and the rows of the image and i represent the multiple acquisitions of each pixel, with $0 < i \leq N$.

When the acquisition of the column is complete, our software performs a discrete Fourier transform of $H(x, y, i)$ for each column to extract a reference angular frequency $\tilde{\omega}(x) = 2\omega_R(x)$ that corresponds to the angular frequency of the incident-light polarization plane (typically 40 to 45 Hz in our experiments), and a reference phase $\tilde{\theta}(x)$. The dependence of $\tilde{\omega}$ and $\tilde{\theta}$ on x is due to the fact that the Fourier transforms are computed on a column-by-column basis, rather than on the entire dataset, to account for variations of the rotation speed of the R-$\lambda/2$ during the acquisition process. This procedure is justified by the observation that, during the acquisition of each column, the rotation speed does not change significantly.

Finally, the program finds the two orthogonal Fourier components of the PMT signal at $2\omega_R(x)$ values and the average value:

$$A^{\sin}_{2\omega}(x, y) = \frac{2}{N} \sum_{i=1}^{N} S(x, y, i) w(i) \sin\left(2i\tilde{\omega}(x) T_L + \tilde{\theta}(x)\right) \tag{1}$$

$$A^{\cos}_{2\omega}(x, y) = \frac{2}{N} \sum_{i=1}^{N} S(x, y, i) w(i) \cos\left(2i\tilde{\omega}(x) T_L + \tilde{\theta}(x)\right) \tag{2}$$

$$A_{dc}(x, y) = \frac{1}{N} \sum_{i=1}^{N} S(x, y, i), \tag{3}$$

where $w(i)$ is a Kaiser-Bessel window function, and calculates the magnitude $A_{2\omega}$ and the phase θ:

$$A_{2\omega}(x, y) = \sqrt{A^{\sin}_{2\omega}(x, y)^2 + A^{\cos}_{2\omega}(x, y)^2} \tag{4}$$

$$\theta(x, y) = \arctan_2\left(A^{\sin}_{2\omega}(x, y), A^{\cos}_{2\omega}(x, y)\right) - \tilde{\theta}(x), \tag{5}$$

where the function $\arctan_2(a, b)$ is the two-argument arctangent function that returns the angle between the positive x-axis of a plane and the point given by the coordinates (a, b). $A_{dc}(x, y)$ contains the information about the density of chemical bond of interest within the PSF volume. To minimize the total acquisition times, this procedure is carried out during the acquisition of the next column of the image. An image based on this function is therefore equivalent to an artifact-free CARS image acquired with the conventional techniques. The magnitude signal $A_{2\omega}(x, y)$ is a measure of how much the raw signal from the (x, y) pixel varies during a rotation of the polarizer and therefore it represents the degree of in-plane anisotropy of the molecular-bond orientation within the point spread function (PSF) volume. The phase value $\theta(x, y)$ is a measure of the orientation of this anisotropy.

Other authors that studied the anysotropy in the lipid membranes [15] with two-photon fluorescence (TPF) microscopy or in textile fibers with CARS [12] exploited a different approach based on the collection of several images each with a slightly different rotation of the polarization plane and subsequent pixel-per-pixel analysis. The acquisition speed of this method is comparable to that of the technique presented here, however with our implementation the visual feedback to the user is much faster as the image is refreshed column per column and also almost all the processing (except for the last column of the image) is performed in parallel with the acquisition. Images are color- and intensity-coded, as described in Ref. [9] and in the legend of Fig. 2 and present bright colors where both a high bond density and a strong anisotropy are present. The hue indicates the predominant direction of the bonds.

A validation of this method was achieved by analysing a structure that presents a very well known and recognisable orientation of the CH_2 bonds, that is a bundle of myelinated nerve fibers in *ex-vivo* mouse (C57BL/6J strain, Jackson Laboratory) sciatic nerve. Lipidic chains are oriented perpendicularly to the membrane and CH_2 bond are therefore parallel to the latter. After the surgery, the nerve explants were incubated in constantly oxygenated (95% O_2 5% CO_2) Krebs-Henseleit Buffer (K3753 Sigma-Aldrich) kept at 30 °C to prevent damages to the fibres.

Figure 2a displays the values of A_{dc}, that is the CARS signal averages through multiple rotation of the polarization plane. Individual myelinated axons can be easily identified. Figure 2b shows the same region depicted in Fig. 2a buth with the color coding described above: the color of the myelin walls changes smoothly accord-

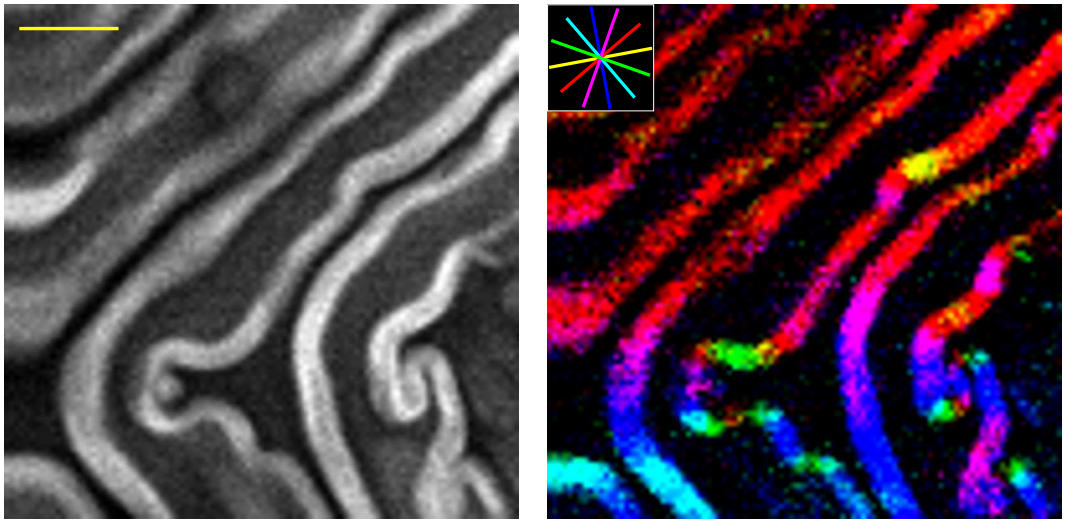

(a) (b)

Fig. 2. Small scale (30 µm × 30 µm, 100 × 100 points) RP-CARS image of myelinated nerve fibers in *ex-vivo* mouse sciatic nerve acquired in epi-direction in about 2 minutes with the presented acquisition method. Scale bar: 6 µm. **(a)** Grayscale image created with the $A_{dc}(x, y)$ signal (averaging pixel-per-pixel the $A_{2\omega}(x, y)$ signal over a complete polarization rotation). The images created in this manner are similar to the traditional CARS images but they are free from polarization artifacts. **(b)** This image is color- and intensity-coded, as described in Ref. [9], by using the HSB color space, where the $A_{2\omega}(x, y)$ signal is mapped onto the brightness channel (this is equivalent to use **(a)** as brightness) and $\theta(x, y)$ onto the hue. Saturation is kept at the maximum value. Inset: color-coding scheme of the hue-mapped orientation.

ing to their local direction, demonstrating that the fast-acquisition method presented here correctly identifies ordered structures and detects the average orientation of the bonds of interest equivalently to the original implementation of this technique [9].

The large-scale, high-resolution capabilities of our approach were tested on a 100 µm thick coronal slice of mouse (C57BL/6J strain, Jackson Laboratory) formaldehyde-fixed brain in the hyppocampal region (bregma: –1.2 mm). The images displayed in Fig. 3 are mosaics made by manually stitching 276 50 × 50 pixels tiles and then processing them with a bi-dimensional band-block Fourier filter (suppressing Fourier components on the vertical and horizontal coordinate axes with 1% tolerance, using ImageJ [16]) to remove the stitching artifacts. In such a large scale image, our method allows visualizing rapidly the in-plane direction of the myelinated nerve fibers. The results are fully consistent with the data in literature [17]: all the major fiber bundles that surround the hyppocampus are clearly recognizable (corpus callosum, cingulum, dorsal fornix, alveus, fimbria and stria medullaris) and visualized with the expected in-plane directions. Each tile column was scanned repeatedly for 320 ms (yielding a total acquisition time of 16 s per tile), corresponding to acquiring the signal from each pixel for approximately 13 revolutions of the polarization plane. Doing an equivalent acquisition pixel-per-pixel with a lock-in amplifier would require a total acquisition time per tile of 800 s, or 60 hours for the entire image (instead of an hour).

3 Conclusions

We presented a novel acquisition technique for RP-CARS. This technique represents a major improvement over the previously presented hardware lock-in approach, leading to a dramatic improvement of the acquisition velocity and therefore making now possible the acquisition of large-scale high spatial resolution RP-CARS images.

In particular, fast RP-CARS imaging of myelin fibers is significant both for the scientific relevance of the myelin sheath from a biological point-of-view and for the clinical importance of the demyelinating diseases. We believe that this approach may significantly impact the study of the brain connectomics (fibers tracking), both in the healthy brain and in pathological states associated with altered neural connectivity. Moreover, it could be useful also to observe the myelin injury process with high temporal resolution and without the confounding use of any dye.

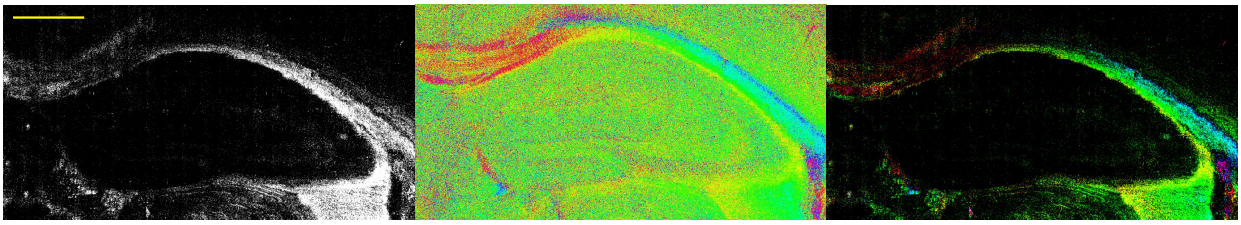

(a) **(b)** **(c)**

Fig. 3. large-scale (2.2 mm × 1.1 mm), high-resolution (pixel size: 2.4 µm × 2.4 µm) RP-CARS image of a coronal section of the mouse brain hyppocampus taken with the presented acquisition method in trans-direction in about 1 hour. Scale bar: 400 µm. **(a)** Grayscale image created mapping $A_{2\omega}(x, y)$ signal as intensity. **(b)** RBG image created mapping $\theta(x, y)$ signal onto the visible color spectrum. The areas that appear dark in **(a)** and in **(c)** (low $A_{2\omega}(x, y)$ signal levels) here appear as random colored due to the noise in $\theta(x, y)$. **(c)** The image is color- and intensity-coded as Fig. 2b and as described in Ref. [9].

References

[1] P.D. Maker and R.W. Terhune. Study of optical effects due to an induced polarization third order in the electric field strength. *Physical Review*, 137(3A):A801, 1965.

[2] Ji-Xin Cheng. Coherent anti-stokes raman scattering microscopy. *Appl. Spectrosc.*, 61:197A–208A, 2007.

[3] Ji-Xin Cheng and X. Sunney Xie. Coherent anti-stokes raman scattering microscopy: instrumentation, theory, and applications. *The Journal of Physical Chemistry B*, 108(3):827–840, 2004.

[4] C.L. Evans, E.O. Potma, M. Puoris' haag, D. Côté, Ch.P. Lin, and X. Sunney Xie. Chemical imaging of tissue in vivo with video-rate coherent anti-stokes raman scattering microscopy. *Proceedings of the National Academy of Sciences of the United States of America*, 102(46):16807–16812, 2005.

[5] C.L. Evans and X. Sunney Xie. Coherent anti-stokes raman scattering microscopy: chemical imaging for biology and medicine. *Annu. Rev. Anal. Chem.*, 1:883–909, 2008.

[6] R.W. Boyd. *Nonlinear optics*. Academic press, 2003.

[7] E Bélanger, S Bégin, S Laffray, Y De Koninck, R Vallée, and D Côté. Quantitative myelin imaging with coherent anti-stokes raman scattering microscopy: alleviating the excitation polarization dependence with circularly polarized laser beams. *Optics express*, 17(21):18419–18432, 2009.

[8] Yan Fu, T Brandon Huff, Han-Wei Wang, Ji-Xin Cheng, and Haifeng Wang. Ex vivo and in vivo imaging of myelin fibers in mouse brain by coherent anti-stokes raman scattering microscopy. *Optics express*, 16(24):19396–19409, 2008.

[9] G. de Vito, A. Bifone, and V. Piazza. Rotating-polarization cars microscopy: combining chemical and molecular orientation sensitivity. *Optics Express*, 20(28):29369–29377, 2012.

[10] F. Munhoz, H. Rigneault, and S. Brasselet. Polarization-resolved four-wave mixing microscopy for structural imaging in thick tissues. *JOSA B*, 29(6):1541–1550, 2012.

[11] V. Le Floc'h, S. Brasselet, J.-F. Roch, and J. Zyss. Monitoring of orientation in molecular ensembles by polarization sensitive nonlinear microscopy. *The Journal of Physical Chemistry B*, 107(45):12403–12410, 2003.

[12] M. Zimmerley, R. Younger, T. Valenton, D. C. Oertel, J.L. Ward, and E.O. Potma. Molecular Orientation in Dry and Hydrated Cellulose Fibers: A Coherent Anti-Stokes Raman Scattering Microscopy Study. *The Journal of Physical Chemistry B*, 114(31): 10200–10208, 2010.

[13] Newport Corporation. Supercontinuum generation in scg-800 photonic crystal fiber. Technical report, Technology and Applications Center Newport Corporation, 2006.

[14] Young Jong Lee, Sapun H Parekh, Yeon Ho Kim, and M.T. Cicerone. Optimized continuum from a photonic crystal fiber for broadband time-resolved coherent anti-stokes raman scattering. *Optics express*, 18(5):4371–9, 2010.

[15] A. Gasecka, Tsai-Jung Han, C. Favard, Bong Rae Cho, and S. Brasselet. Quantitative imaging of molecular order in lipid membranes using two-photon fluorescence polarimetry. *Biophysical journal*, 97(10):2854–2862, 2009.

[16] W.S. Rasband. Imagej. U. S. National Institutes of Health, Bethesda, Maryland, USA http://imagej.nih.gov/ij/, 1997-2012.

[17] G. Paxinos. *The mouse brain in stereotaxic coordinates*. Academic press, 2004.

Received April 10, 2013; accepted October 3, 2013.